Journal of Colloid and Interface Science 606 (2022) 1974–1982

Contents lists available at ScienceDirect

Journal of Colloid and Interface Science

journal homepage: www.elsevier.com/locate/jcis

Colloid-like solution behavior of computationally designed coiled coil bundlemers

Nairiti J. Sinha [a,b], Rui Guo [c], Rajkumar Misra [a], Jeffrey Fagan [b], Antonio Faraone [b], Christopher J. Kloxin [d], Jeffery G. Saven [c], Grethe V. Jensen [b,d,1,*], Darrin J. Pochan [a,*]

[a] Department of Materials Science and Engineering, University of Delaware, Newark, DE, USA
[b] NIST Center for Neutron Research (NCNR), National Institute of Standards & Technology (NIST), Gaithersburg, MD, USA
[c] Department of Chemistry, University of Pennsylvania, Philadelphia, PA, USA
[d] Department of Chemical and Biomolecular Engineering, University of Delaware, Newark, DE, USA

HIGHLIGHTS

- Bundlemers are model globular protein mimicking colloidal particles.
- Bundlemers can be computationally desinged to display desired net charge and pattern.
- Bundlemers display a balance of attraction and repulsion interactions.

GRAPHICAL ABSTRACT

Bundlemer (grey cylinders) solution structure at various concentrations (C) and length scales (Q^{-1}) is dictated by short-range attraction (green) and long-range repulsion (yellow) interactions.

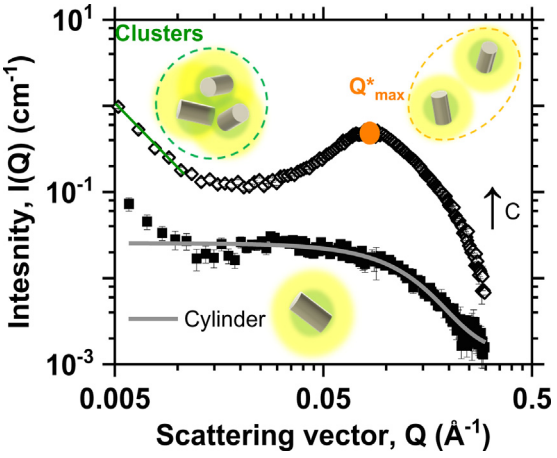

ARTICLE INFO

Article history:
Received 7 April 2021
Revised 23 September 2021
Accepted 28 September 2021
Available online 1 October 2021

Keywords:
Bundlemer

ABSTRACT

The use of isotropic potential models of simple colloids for describing complex protein–protein interactions is a topic of ongoing debate in the biophysical community. This contention stems from the unavailability of synthetic protein-like model particles that are amenable to systematic experimental characterization. In this article, we test the utility of colloidal theory to capture the solution structure, interactions and dynamics of novel globular protein-mimicking, computationally designed peptide assemblies called bundlemers that are programmable model systems at the intersection of colloids and proteins. Small-angle neutron scattering (SANS) measurements of semi-dilute bundlemer solutions in low and high ionic strength solution indicate that bundlemers interact locally via repulsive

* Corresponding authors at: NIST Center for Neutron Research (NCNR), National Institute of Standards & Technology (NIST), Gaithersburg, MD, USA (G.V. Jensen). Department of Materials Science and Engineering, University of Delaware, Newark, DE, USA (Darrin J. Pochan).
E-mail addresses: gvj@teknologisk.dk (G.V. Jensen), pochan@udel.edu (D.J. Pochan).
[1] present address: Danish Technological Institute, Tåstrup, Denmark.

https://doi.org/10.1016/j.jcis.2021.09.184

Computational design
Protein–protein interactions
Colloids
Small-angle neutron scattering (SANS)
Neutron spin echo (NSE)

interactions that can be described by a screened repulsive potential. We also present neutron spin echo (NSE) spectroscopy results that show high-*Q* freely-diffusive dynamics of bundlemers. Importantly, formation of clusters due to short-range attractive, inter-bundlemer interactions is observed in SANS even at dilute bundlemer concentrations, which is indicative of the complexity of the bundlemer charged surface. The similarities and differences between bundlemers and simple colloidal as well as complex protein–protein interactions is discussed in detail.

1. Introduction

Nanoparticles ranging from simple colloids to complex proteins have been extensively investigated for their solution behavior and dynamics.[1–7] There is a significant technological precedent and need to systematically investigate the complex protein–protein interaction landscape due to widespread protein use in therapeutic formulations and to understand natural protein hierarchical assembly, crystallization, and function.[8,9] Although colloidal theory was initially used to describe proteins in solution, colloidal and protein solution behavior and assembly have branched into distinct material engineering fields.[5,10,11] Experiments increasingly indicate that colloidal theory based on simple isotropic interaction potentials is insufficient to capture the subtleties of the multi-charged, solvent-exposed surfaces and the resulting non-trivial anisotropic interactions in protein systems. [11,12] Discovery of new model systems for proteins is needed, not only to enable characterization of the sequence-driven protein–protein interaction landscape at the fundamental level but also to facilitate the informed construction of hierarchically self-assembled biomaterials made with designed protein systems.

Previously, we have presented the synthesis and self-assembly of computationally designed and solution assembled antiparallel, homotetrameric coiled coils called 'bundlemers'. [13–16] The non-natural globular protein-like cylindrical bundlemers are compact, robust assemblies of four identical, computationally predicted peptide sequences. The hydrophobic residues form the bundlemer core and solvent-exposed side-chains are designed *in silico* to display a desired net charge on its surface. The side-chains on the solvent exposed bundlemer surface exhibit the inherent D_2 symmetry and supra-helical pitch of the antiparallel homotetrameric bundlemer design. [13] Thus, the computationally designed bundlemer mimics the complexity of a small, natural globular protein and therefore, provides a model protein template for the study of solution structure and dynamics.

Previously, we characterized the size and shape of the bundlemer unit using small-angle neutron scattering (SANS), confirming its cylindrical shape with cross-sectional and length dimensions of approximately 20 Å and 40 Å, respectively. [14] We also attempted to characterize the solution behavior of the net-charged bundlemers in buffered solution. [14] However, the inter-bundlemer interactions were complicated by the mixed electrolyte ions present in the buffer and also by the nonzero net-charge on the bundlemer. In this article, we have simplified the bundlemer system by investigating a newly designed bundlemer peptide sequence with zero net charge underlying its inter-bundlemer interactions and dynamics in pure solvent (low-ionic strength solution) and in the dilute to semi-dilute concentration-regime. We studied a new, computationally designed peptide sequence **peptide_1** that is designed to carry a net-neutral charge at pH 7.0. The theoretical neutral net-charge is a result of an equal number of oppositely charged solvent-exposed side-chains in the non-natural peptide sequence. We employed SANS to measure the solution nanostructure and neutron spin echo (NSE) spectroscopy [6,7] to gain insight into the local dynamics of the bundlemers in low-ionic strength solution, 0.05 mol/L sodium chloride (salt) and 0.025 mol/L phosphate buffer, pH 7. Together, SANS and NSE reveal that the bundlemers exist as repulsive colloids in solution but also have some fraction forming bundlemer clusters. The results are compared to similar studies of globular proteins and colloids.

2. Materials and methods

2.1. Computational design of peptide_1

The computational design of **peptide_1** sequence was performed as follows. A *de novo* designed, 29-residue, antiparallel, tetra-helical backbone structure was used for design of constituent peptides. Details of the design of the structure and hydrophobic core have been discussed previously. [13,15] The bundle structure and its hydrophobic interior core have been shown to be to be robust with respect to variation of exterior residues. The exterior residues were redesigned so as to modify the total charge of the sequence, opting for a sequence that is expected to have zero net charge at pH 7. In the design, we began with the sequence labeled BNDL_1 (DEEIRRMAEEIRQMAERIQQMAEQIYQEA-NH_2) in Zhang et al, [13] which has an original total expected charge (in units of the electron charge) of −3 per peptide. The computational design approach [13,17–21] yields the probabilities of amino acids at 18 variable exterior positions and was applied to identify amino acid substitutions that modulate the overall expected charge. Mutations are identified one at a time, using repeated calculations, ultimately resulting in the sequence **peptide_1** which has three glutamine residues exchanged for lysine and is expected to have a net charge of zero at pH 7 (DEEIRRMAEEIRKMAERIKQMAEQIYKEA-NH_2). For more information, refer to *supplementary information* section 1.1.

2.2. Synthesis and purification of bundlemers

Peptide_1 with a free *N*-terminus and amidated C-terminus was synthesized as reported previously. [13–15,22] The detailed protocol is given in *supplementary information* section 1.2. Peptides were synthesized at a 0.25×10^{-3} mol scale via microwave-assisted fmoc-based solid-phase peptide synthesis (fmoc-SPPS) on a CEM Liberty Blue™ Automated Microwave Peptide Synthesizer. [23] Rink-amide resin (ChemPep) that yields an amidated C-terminus after the final cleaving step was utilized for all syntheses. The peptide elution peak after Reverse-Phase High-Performance Liquid Chromatography (HPLC) purification was collected and checked for the correct molecular weight using electron-spray ionization mass spectroscopy (ESI-MS) on Waters Xevo G2-XS QTof Quadrupole Time-of-Flight Mass Spectrometry instrument (see *supplementary information* for ESI-MS results).

2.3. Characterization

Initial characterization of the bundlemer to probe its α-helical secondary structure was performed using Circular Dichroism spectroscopy (CD), followed by analytical ultracentrifugation (AUC) and

Dynamic Light Scattering (DLS) that were used to confirm the formation of homotetrameric bundlemers (see *supplementary information* for details of techniques and results). The solution structure and bundlemer dynamics were characterized using a SANS and NSE as described below. Unless otherwise stated, error bars in all the data points and uncertainty in mean value of fitted model parameters represent ± 1σ where σ is one standard deviation.

2.3.1. Small-angle neutron scattering (SANS)

The sample with the highest peptide concentration was dialyzed extensively against fresh deuterium oxide (D_2O) and measured first. Dilution to lower concentrations was performed using fresh deuterium oxide (D_2O) for subsequent measurements. The same steps were performed for peptide samples prepared in 0.05 mol/L sodium chloride and 0.025 mol/L phosphate buffer (ionic strength ≈ 0.05 mol/L). At each dilution step, the samples were degassed (5 min) and sonicated (10 min) in a sonication bath at 22 °C and rested for at least 30 min prior to SANS measurement. All samples had a pD ~ 6 as measured using Hydrion pH paper. SANS experiments were performed at the National Institute of Standards and Technology (NIST) Center for Neutron Research, Gaithersburg, Maryland, USA. The CHRNS vSANS beamline was utilized for conducting the measurements. A wavelength of 6 Å of cold neutrons with a wavelength spread of 12 % was employed. A Q-range of 0.004 $Å^{-1}$ < Q < 0.3 $Å^{-1}$ was used where Q is the momentum transfer of the scattered neutron and is defined as $Q = (4\pi \sin\theta)/\lambda$, where λ is the wavelength of the incoming beam of neutrons and 2θ is the scattering angle. All scattering data were reduced using NIST NCNR's IgorPro data reduction software and methods. [24] For analyses of SANS data, SasView analysis software was utilized. [25] Best fit results with the lowest reduced chi-squared (χ^2_R) values were obtained after multiple fitting routines. The mean and standard deviation (σ) for each fit parameter was calculated.

2.3.2. Neutron spin echo (NSE)

Experiments were performed at the CHRNS NSE instrument at National Institute of Standards and Technology (NIST) Center for Neutron Research, Gaithersburg, Maryland, USA. A wavelength of 6 and 8 Å of cold neutrons with a wavelength spread of 20 % was employed to cover a Q-range of 0.03–0.13 $Å^{-1}$ and Fourier time range of 0.05–45 ns. The neutron echo was measured for Φ = 0.4%, where Φ is the volume percent of the bundlemer sample in pure D_2O at 22 °C, 45 °C and 65 °C and in 0.05 mol/L sodium chloride at 22 °C. All echo data were reduced using NIST NCNR's Dave data reduction and analysis software. [26] Best fit results with the lowest possible reduced chi-squared values were obtained and mean and standard deviation (σ) for each fit parameter was calculated.

2.4. Theory

2.4.1. SANS data modeling

In a SANS experiment, the scattering intensity *I(Q)* from a solution of monodisperse scattering species is measured as a function of the scattering vector Q which is described by the equation: [27,28]

$$I(Q) = nV_p^2(\rho_p - \rho_s)^2 P(Q).(1 - \beta(Q)[S(Q) - 1]) \quad (1)$$

Where, n is the number density of scatterers having a molecular volume V_p and scattering length density (SLD) ρ_p dispersed in a solvent with SLD ρ_s. It is apparent from Eq. (1) that the contrast term $(\rho_p - \rho_s)^2$ is correlated with concentration of scatterers n. SLD values were calculated from atomic coherent scattering length density allowing for the bundlemer concentration to be an independent fit parameter (see *supplementary information* for calculation). Since the bundlemers are cylinders with radius, *R*, and length, *L*, and have a small aspect ratio, the shape and size of the scatterers is captured in the form factor *P(Q)* averaged over all particle orientations, given by:

$$P_{cyl}(Q) = < A^2(Q) > = \int_0^{\pi/2} A^2(Q,\alpha) sin\alpha d\alpha \quad (2)$$

Here, *A(Q)* is the amplitude function of a cylinder, given by:

$$A(Q,\alpha) = \frac{sin(QLcos(\alpha)/2)}{QLcos(\alpha)/2} \cdot \frac{2J_1(QRsin(\alpha))}{QRsin(\alpha)} \quad (3)$$

We fit the radius, *R* and length, *L* of the cylinder, and use the beta approximation factor, $\beta(Q) = < A(Q) >^2 / < A^2(Q) >$, to account for the anisotropic shape of the bundlemers under the assumption that the relative bundlemer nanocylinder orientations are independent. [28]

At high concentrations, inter-bundlemer interactions are described by the structure factor, *S(Q)*. We have utilized both the Effective Hard Sphere (EHS) and the Hayter-Penfold (HP) *S(Q)* in SasView analysis software to model the interaction peak in the high concentration *I(Q)* regime of the bundlemers. [25] The EHS *S(Q)* uses a Percus-Yevick closure to the Ornstein-Zernike (OZ) equation and describes hard-core inter-particle interactions *U* at inter-particle distances *r* via the following expression: [29]

$$U_{EHS}(r) = \infty r \le R_{eff,EHS}$$

$$= 0 r > R_{eff,EHS} \quad (4)$$

Here, $R_{eff,EHS}$ is the effective radius of the particle which is extracted from the SANS data for this model. In contrast, the HP *S(Q)* incorporates a Yukawa potential to describe screened columbic repulsion between particles and uses a mean-spherical approximation closure to the OZ equation. [30,31]

$$U_{HP}(r) = \infty r \le R_{eff,HP}$$

$$= U_o \frac{R_{eff}}{r} exp\left[-\lambda^{-1}(r - R_{eff})\right] r > R_{eff,HP} \quad (5)$$

Here, λ is the Debye - Hückel screening length given by $\lambda = \left(\frac{\varepsilon\varepsilon_o k_B T}{\sum c_j Z_j^2}\right)^{-2}$ (where k_B is the Boltzmann constant and T = 295.15 K is the temperature) and U_o is the depth of the potential given by $U_o = q'/(4\pi\varepsilon\varepsilon_o R_{eff,HP})$. Thus, the apparent charge carried by the interacting particles, q', in a solvent of dielectric constant ε and having a total ionic strength $\frac{1}{2}\sum c_j Z_j^2$ (molar concentration of ions, c_j having a charge valency, Z_j) can be extracted using the HP model. For salt-free measurements, the ionic strength is contributed by the charged peptide itself since ionic strength of added electrolyte is zero, and the effective radius, $R_{eff,HP}$ and apparent charge on peptide, q' can be extracted. Details of all fit parameters are given in the supplementary information.

2.4.2. NSE data modeling

For analyses of the intermediate scattering function, *I(Q,t)*, calculated from the background-subtracted neutron spin echo data, a single exponential decay expression with respect to Fourier time *t* was utilized: [7]

$$\frac{I(Q,t)}{I(Q,0)} = exp[-\Gamma(Q)t] \quad (6)$$

In this expression, Γ is the first cumulant of dynamic correlations, also called the decay rate. For freely diffusive particles, the decay rate is a function of scattering vector Q as

$$\Gamma(Q) = DQ^2 \quad (7)$$

Here, the proportionality constant D is the diffusion coefficient of an effective spherical particle of radius a diffusing freely in a solvent having viscosity η at a temperature T, which is given by the Stokes-Einstein equation. [7]

$$D = \frac{k_B T}{6\pi\eta a} \tag{8}$$

where, k_B is the Boltzmann constant.

3. Results and discussion

The *in silico* designability of the bundlemer was exploited to create a new peptide sequence, **peptide_1,** based on an original sequence designed by Zhang et al. [13] The **peptide_1** sequence was characterized for the formation of a monodisperse, α-helical, and homotetrameric coiled coil, or bundlemer, assembly using a combination of spectroscopy techniques that are summarized in **Fig. S1** in *supplementary information*. **Peptide_1** sequence includes 8 negatively charged residues and 8 positively charged residues on solvent exposed sites, which results in a complex surface charge pattern and charge neutrality of the resulting homotetrameric bundlemer assembly around pH 7, with an estimated isoelectric point at 7.2. (The net charge on the bundlemer forming peptide at various pH that is calculated using the *pKa* of dissociable amino acid side chains is provided in the *supplementary information*). We characterized the solution nanoscale structure of the bundlemers in pure D_2O by performing a dilution series measurement using SANS. Throughout this article, the concentration (Φ) is reported in volume fraction which was calculated by the relation $\Phi = m/(V\delta_p)$ where m is the gravimetric mass of peptide, V is the solution volume, and δ_p is the average density of proteins (δ_p = 1.35 g/ml) [32]. The apparent structure factor $S'(Q) = (I(Q)-B)/(I_0\, P(Q))$ (where $I_0 = nV_p^2$ is the pre-factor term in Eq. (1) and B is the background scattering), as a function of scattering vector, Q, is plotted in Fig. 1**A**. Here P(Q) is the cylinder form factor fit to the SANS data of bundlemer sample containing lowest peptide concentration (Φ = 0.2 %).

Initial analysis of the apparent structure factor $S'(Q)$ data reveals two important features. First, upon increasing the bundlemer concentration, a maximum and minimum pair is apparent in the high-Q and mid-Q region, respectively, indicated by arrows in Fig. 1**A**. The position of the scattering vector, Q^*, at the maximum (Q^*_{max}) shifts to higher Q with increasing concentration and scales as the one-third power of concentration ($Q^*_{max} \sim \Phi^{1/3}$) (see Fig. 1**B**). This behavior is characteristic of particles interacting via excluded volume interactions, which can be modeled using effective hard-sphere or screened columbic repulsion potentials. [33,34] Second, an upturn in intensity is recorded at low-Q for all concentrations wherein $S'(Q < Q_{min}^*) \sim Q^{-2}$. This low-Q feature indicates the formation of bundlemer clusters. A low-Q upturn in intensity was also recorded in our previous study of inter-bundlemer interactions which we attributed to the formation of soluble aggregates of bundlemers. [14]

Since the low-Q intensity is effectively decoupled from the mid- and high-Q intensity, we can model the $I(Q)$ data in the mid- to high-Q range using the Hayter-Penfold (HP) structure factor model coupled with a cylinder form factor, which is described by Eq. (1) (Fig. 2**A** and Fig. 2**B, Fig. S2** in *supplementary information* for goodness of fit). The effective hard sphere (EHS) structure factor is also employed for comparison. For both models, a low-Q cutoff of Q^*_{min} = 0.016 Å^{-1} was employed. For the lowest concentration in which negligible inter-particle interactions are observed ($Q^*_{min} \approx Q^*_{max}$), the cylinder form factor ($P_{cyl}(Q)$) was used to model the SANS data (i.e., $S(Q)$ = 1 in Eq. (1)). Dimensions of the cylinder were extracted as fitted values of the radius, R = (11.5 ± 0.4) Å, and length, L = (37.0 ± 1.5) Å. These values are in good agreement with the computational model structures and our previously reported results for bundlemers. [13,14,22]

At higher bundlemer concentrations, inter-bundlemer interactions dominate the $I(Q)$ data and $S(Q) \neq 1$. Analyses indicate that the inter-bundlemer interactions can be modeled using both the EHS model and the HP model. The fits to the EHS model via Eq. (4) yield the effective radius of the nanoparticle, $R_{eff,\ EHS}$, and the volume fraction of particles, Φ_{EHS}, and the fits to HP model yield the effective radius. $R_{eff,\ HP}$, volume fraction. Φ_{HP}, and an apparent net charge on the bundlemer, q' (see Eq. (5) and schematic in Fig. 2**A**). Here, the bundlemer volume fraction was also fitted using EHS and HP models and compared to the true volume fraction of peptides in solution, Φ in Fig. 2**C**.

Comparison of fit results indicate that the HP model predicts the volume fraction correctly and, as noted above, is also the phenomenologically accurate model for interacting bundlemers in solution (refer to Fig. 2**C and 2D**). The HP model fits yield the expected values of bundlemer volume fraction and an average effective radius $R_{eff,\ HP}$ = 21.0 ± 0.8 Å. This value is twice the cylindrical radius of the bundlemer and half the length of the bundlemer ($R_{eff,\ HP} \approx 2R \approx L/2$). Thus, the bundlemers can be approximated as spherical particles of diameter ≈ L. Also, the HP model yielded an apparent charge on the bundlemer, $q' \approx 7\ e$,

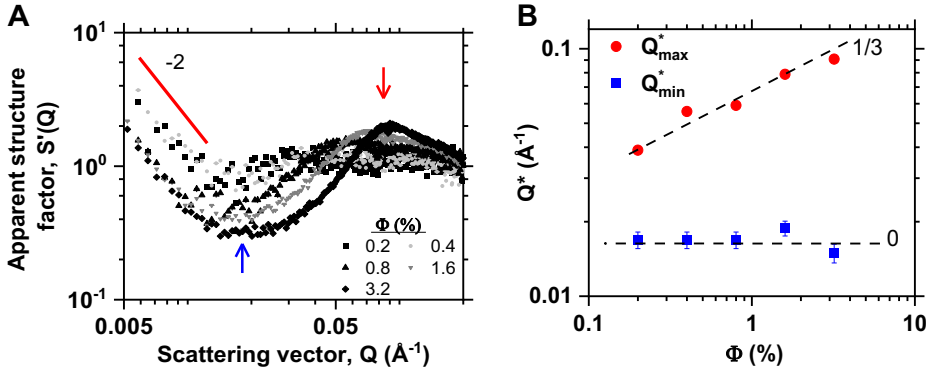

Fig. 1. (A) Small-Angle Neutron Scattering (SANS) apparent structure factor $S'(Q)$ plotted versus scattering vector, Q, for a dilution-series of bundlemers dispersed in pure deuterium oxide (D_2O). The concentration is expressed as volume percent of bundlemers, Φ. The red arrow indicates the position of the maximum and blue arrow indicates the position of the minimum in the mid- to high-Q range for the 3.2 % sample. The red solid line is indicative of a slope of −2 on the log–log plot. **(B)** Plot of scattering vector at the maximum (Q^*_{max}) and at the minimum (Q^*_{min}) as a function of bundlemer concentration. The black dashed lines have slopes indicated. (For interpretation of the references to colour in this figure legend, the reader is referred to the web version of this article.)

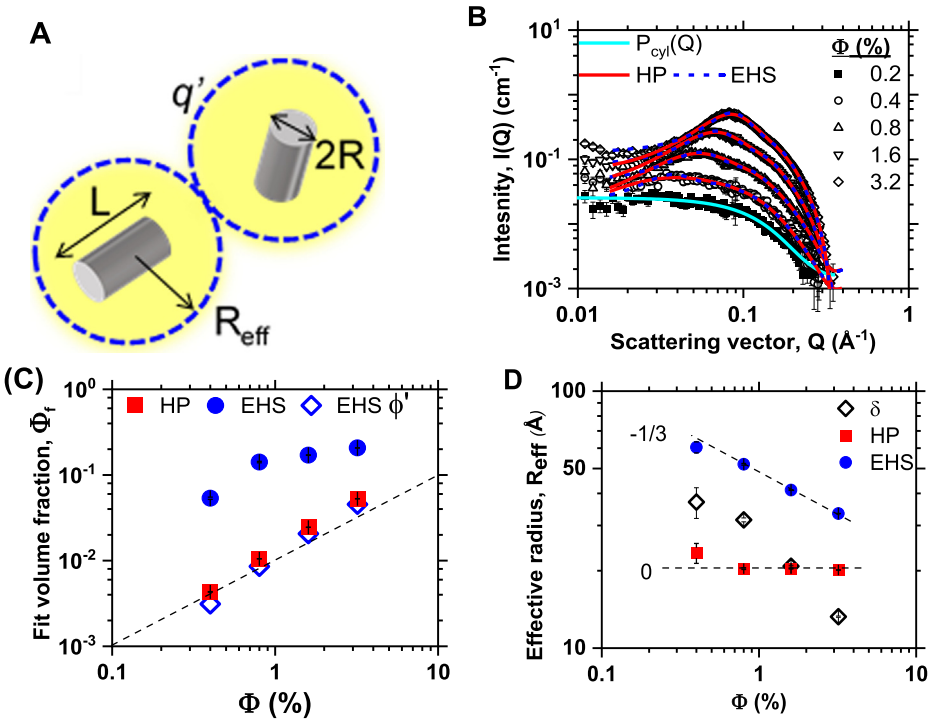

Fig. 2. **(A)** Schematic of interacting bundlemers depicted as grey cylinders having a radius R and length L carrying an apparent net charge q' and interacting in solution at an effective distance R_{eff}. **(B)** Fits to SANS data using cylinder form factor $P(Q)$ and either a Hayter-Penfold repulsive (HP, solid red line) or Effective Hard Sphere (EHS, blue dashed line) structure factor. **(C)** Comparison of fitted value of volume fraction between the HP and EHS models. The scaled volume fraction for EHS model, Φ', is also plotted for comparison. The dashed black line represents the true volume fraction. **(D)** Fitted effective radius with the HP and EHS models. The thickness of the electric double layer, δ is also shown. The error in δ was calculated by error propagation. The dashed lines have slopes indicated on the plot. (For interpretation of the references to colour in this figure legend, the reader is referred to the web version of this article.)

where $e = 1.6 \times 10^{-19}$C is the columbic charge on an electron. The fitted value of q' was mildly sensitive to the low-Q cutoff for the HP fit, which is a consequence of the bundlemer cluster scattering at low-Q,. Also, it is important to note here that the q' is the net charge on the homotetrameric bundlemer i.e. the net charge on each peptide is $q'/4$. Given that the $pD \approx 5$–6 of unbuffered peptide solution in low ionic strength D_2O solvent, one would expect each peptide in the bundlemer to carry a slight positive charge of up to $\approx 2\ e$ based on net-charge calculations (see *supplementary information* for net charge versus pH plot). Hence, the fitted q' is not a large, unexpected value. Thus, the charged side-chains have dissociated nonuniformly in the unbuffered, low-ionic strength solvent, which is a consequence of the multi-charged local character of proteins. [35] Furthermore, counter ions, slight changes in pH (especially for the D & E residues near the N-terminus), as well as modulation of some of the *pKa's* of residues all may play a role in determining the net charge on the bundlemer.

A comparison with the EHS model yields some classic colloidal behavior expected when this simplified potential is used to fit SANS data of locally repulsive particles. [36] Firstly, EHS model overestimates the volume fraction of bundlemers (See Fig. 2**C**). This result is expected for repulsive particles since the EHS model is fitting an $R_{eff,\ EHS}$ that is essentially the effective range of the bundlemer repulsion potential which is larger than the actual bundlemer size. Thus, the fitted effective radius scales as $R_{eff,\ EHS} \sim \Phi^{1/3}$, a trend that is expected of EHS fits to a dilute solution of repulsive colloidal particles. [11] A scaled volume fraction Φ' can be calculated via the relation:

$$\Phi' = \Phi_{eff,EHS}\left(\frac{R_{eff,HP}}{R_{eff,EHS}}\right)^3$$

This new scaled volume fraction for the EHS model now agrees well with the expected volume fraction (Fig. 2**C**). An effective thickness of the electric double layer δ can also be extracted using the relation: $\delta = R_{eff,EHS} - R_{eff,HP}$, which decreases with increasing concentration (Fig. 2**D**). This trend in the effective thickness manifests due to an increase in overlap of electric double layers as bundlemer concentration increases, which results in the correlation peak. Interestingly, at the lowest concentrations, the electric double layer thickness is approximately three times the bundlemer size, which alludes to a loosely bound counterion cloud in low ionic strength solution.

The fits of the colloidal models to the mid- and high-Q scattering data indicate that they are robust descriptors of the local structure of the bundlemers. However, a single excluded volume model cannot capture the scattering intensity as Q approaches Q^*_{min}. The low-Q intensity upturn at $Q < Q^*_{min}$ suggests that scattering from larger bundlemer clusters dominates in this Q-regime as discussed above and has been reported in the literature. [3,34,37,38] In case of bundlemers dissolved in D_2O, sample preparation technique and thermal history was found to directly impact the intensity in the low-Q upturn (see Fig. 3). Here, freshly prepared samples refer to peptide solution that was prepared by suspending newly synthesized and lyophilized peptide in pure D_2O solvent for the first time. Specifically, the cluster size of freshly prepared samples varied between different samples (comparing low-Q upturn between Fig. 3**A, B and C**). Furthermore, we did not record significant changes in low-Q intensity between freshly prepared and aged samples. These results indicate that there exists an underlying short-range attraction between bundlemers that results in stable, long-lived clusters that do not readily break-up on dilution during the course of the SANS experiments. We did not attempt to model

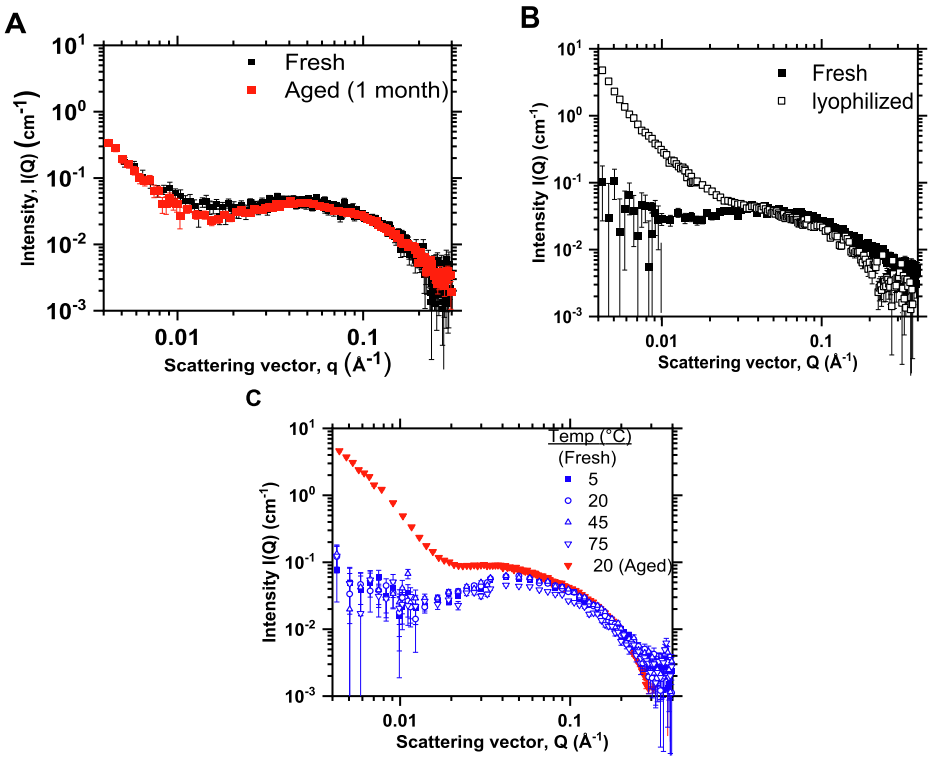

Fig. 3. Impact of sample preparation history on bundlemer solution structure. Three different samples containing a 0.04 vol fraction of the bundlemer solution was investigated after subjecting them to different aging histories using SANS. **(A)** Sample aged on benchtop at ambient temperature for 1 month (red squares) were comparable to freshly prepared samples (black squares). The freshly prepared sample had a slightly higher low-Q upturn than in samples in (B) and (C), indicating sensitivity to initial sample preparation environment. **(B)** Sample prepared from re-lyophilized and resuspended peptides (open black squares) contained more aggregates in comparison to the original freshly prepared sample (solid black squares) as indicated by the increase in low-Q intensity. **(C)** SANS curves of temperature scans of a freshly prepared sample (blue symbols) and the same sample after cooling and aging for 1 week (red inverted triangles). The initial heat treatment of bundlemers was performed for 1 h at each temperature before SANS data was collected. Heating did not impact the coherent scattering intensity which corroborates the robustness of the bundlemer structure. The low-*Q* upturn in the same sample after cooling to room temperature and aging confirmed the formation of large aggregates in the sample. (For interpretation of the references to colour in this figure legend, the reader is referred to the web version of this article.)

the low-*Q* intensity, although a generic Lorentzian expression has been used previously to model this feature. [14] Signature of bundlemer cluster formation was also observed in DLS and AUC measurements on bundlemer solutions, albeit under slightly different solution conditions (see **Fig. S1(D) and S1(E)** in *supplementary information*).

Evidence of individual bundlemers diffusing freely in solution was confirmed using NSE measurements for bundlemer sample with $\Phi = 0.004$, for 0.02 Å^{-1} < Q < 0.2 Å^{-1} and at different temperatures. Here, the intermediate scattering functions, $I(Q,t)$, were fitted using a single exponential expression (Eq. (6)) that yielded the first cumulant, i.e., decay rate, Γ, which followed the expected Q^2 scaling behavior for freely diffusive particles that was temperature dependent (Fig. 4**A,** see supplemental information for NSE data and analysis protocol). [7] The reduced decay rate $(\Gamma\eta T^{-1})$, which is expected to follow $\Gamma\eta T^{-1} = (k_B/6\pi\ a)Q^2$ via combination of Eq. (7) and Eq. (8) was calculated and the resulting curve collapsed onto a single line on a log–log plot as expected (shown in Fig. 4**B**). The intercept of the fit to the data in Fig. 4**B** was utilized to extract the hydrodynamic radius, *a*, of bundlemers since $\log(\Gamma\eta T^{-1}) = \log(k_B/6\pi\ a) + 2\log(Q)$.

A bundlemer hydrodynamic radius of $a = 21 \pm 1$ Å was extracted for bundlemers in low ionic strength solution. The extracted hydrodynamic radius is similar to the effective radius fit using the HP model, $R_{eff,\ HP} = 21$ Å and is similar to the size of the bundlemer extracted from form factor fits to SANS data. Interestingly, a deviation from the $\Gamma \sim Q^2$ behavior is recorded at the lowest-Q data point. For bundlemers at this volume fraction, a correlation hole corresponding to the HP *S(Q)* manifests at $Q < 0.05$ Å^{-1} in Fig. 1, suggesting that the deviation may be related to the inter-bundlemer interactions. However, more data points are required to definitively explain the cause of this deviation and is not explored further in this article. Nevertheless, we can infer using the NSE results that bundlemers are behaving as freely diffusing colloids in solution at distances corresponding to high-Q values.

A final confirmation of the presence of long-range repulsive colloidal inter-bundlemer interactions was gained by measuring the bundlemer solution structure in the presence of electrolytes, specifically 0.05 mol/L ionic strength monovalent sodium chloride salt (unbuffered) and 0.025 mol/L multivalent sodium phosphate buffer, pH 7.0 which has an inherent ionic strength of 0.05 mol/L. The SANS results for the bundlemers in high ionic strength solution are shown in Fig. 5**A and C**. As expected for charged colloidal particles, addition of salt resulted in the suppression of the intensity minima ($I(Q^*_{min})$) due to screening of charged side-chains by counter-ions. [39,40] The extent of screening depends on the ratio of salt counterions to dissociable bundlemer species. Consequently, form factor-like scattering was recovered at lower bundlemer concentrations whereas partially screened interactions were apparent at higher bundlemer concentrations. NSE of the bundlemers in monovalent salt solution for bundlemer solution having 0.004 vol fraction also showed a slowing down of the bundlemers by ≈ 15 % (see Fig. 5**B**). In this sample, the *S(Q)* is effectively 1 in the *Q*-range probed in NSE due to screened charges. The difference in decay rate data cannot be explained by the negligible viscosity change that is expected on addition of 0.05 mol/L sodium chloride

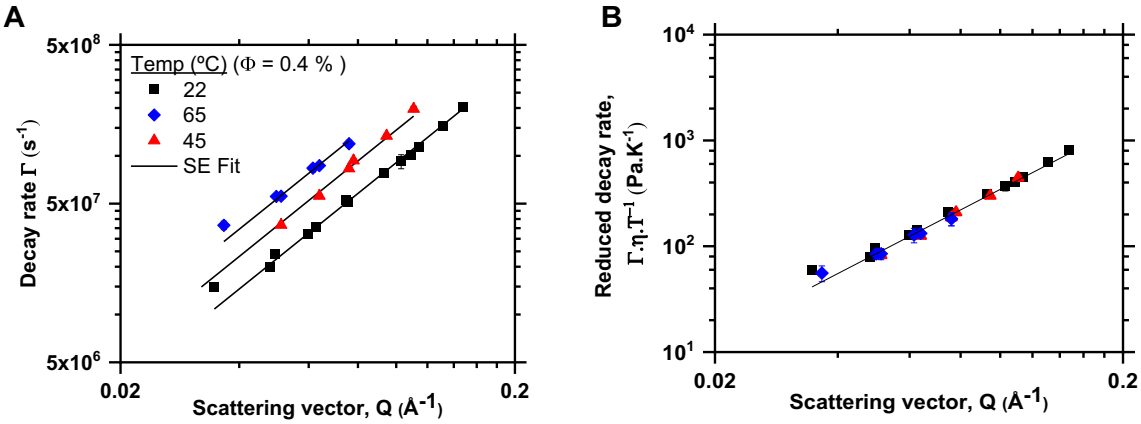

Fig. 4. Neutron Spin Echo (NSE) results for 0.004 vol fraction of bundlemers in in pure deuterium oxide. **(A)** Results for decay rate, Γ versus scattering vector, Q for a temperature series of bundlemers. Fits to $\Gamma = D\,Q^2$ (see Eq. (7) and Eq. (8)) are plotted as black lines. **(B)** Reduced decay rate $\Gamma\eta T^{-1}$ versus scattering vector, Q plot showing the data collapses to a single curve. Black line is fit to the data.

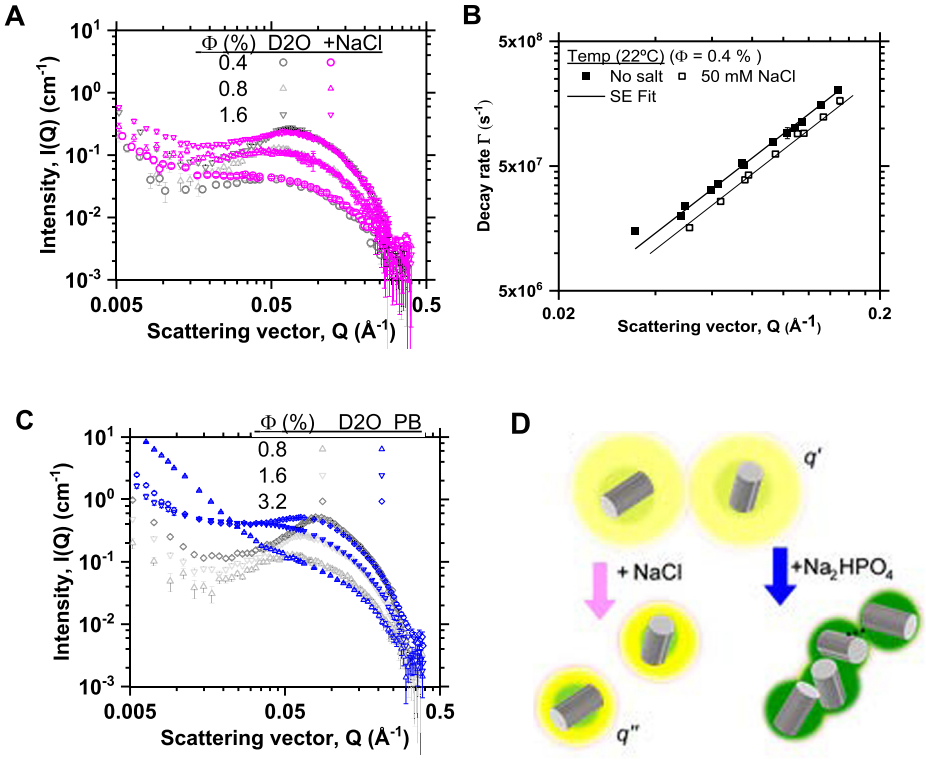

Fig. 5. **(A)** Small-angle neutron scattering (SANS) data for dilution series of bundlemers in 0.05 mol/L sodium chloride solution compared with corresponding data in pure deuterium oxide. **(B)** Neutron spin echo (NSE) data for 0.004 vol fraction bundlemer solution in pure deuterium oxide and in 0.05 mol/L sodium chloride. The decay rate, Γ is plotted against scattering vector, Q and fit to the scaling law $\Gamma = D\,Q^2$ (Eq. (7) and Eq. (8)) represented by black lines for corresponding data. **(C)** SANS data for bundlemers in pH 7 phosphate buffer having an ionic strength of 0.05 mol/L compared with corresponding data in pure deuterium oxide. **(D)** Schematic of impact of electrolyte ions on inter-bundlemer (grey cylinder) interactions. The green halo around the bundlemers represent short-range attraction interactions and the yellow halo around the bundlemers represent long-range repulsive interactions. On addition of monovalent salt, long-range repulsive interactions are screened whereas on addition of multivalent anions, the short-range attractive interactions are further enhanced via formation of inter-bundlemer ionic crosslinks (black dashed line). (For interpretation of the references to colour in this figure legend, the reader is referred to the web version of this article.)

salt. [41] The corresponding hydrodynamic radius of bundlemers extracted using a combination of Eq. (7) and Eq. (8) in salt solution is a = 26 ± 1 Å. The additional thickness of ≈ 5 Å in the salt case in comparison to the pure solvent case can be attributed to the presence of an electrolyte dense counter-ion cloud. The associated salt ions make the bundlemers bulkier which diffuse slower than those dissolved in a low-ionic strength solution.

Suspension of bundlemers dissolved in phosphate buffer (25 mM, pH 7.0) having the same ionic strength as the monovalent salt solution showed significantly denser cluster aggregates at similar bundlemer concentrations. This was evident by the stronger low-Q scattering intensity (see Fig. 5**C**). Phosphate buffer has an equal concentration of mono- and dibasic phosphate anions in pH 7 buffer formulation. While the sodium and phosphate ions

screen the long-range repulsive inter-bundlemer interactions, the dibasic phosphate ions can provide short-range attractive interactions by acting as ionic crosslinks between bundlemers, consequently increasing their tendency to aggregate into clusters even at low bundlemer concentrations (see schematic in Fig. 5**D**). This type of multivalent ion crosslinking is a common observance in the study of protein solution behavior. [42,43] At even higher ionic strength solutions in which inter-bundlemer repulsion is completely screened, they behave as fully attractive colloidal systems in which 'salting-out' or phase separation of bundlemers is observed (see *supplementary information* **Fig. S4**). This phenomenon has also been observed in protein systems in which careful consideration of multivalent ion type and concentration is required to avoid runaway protein aggregation when choosing excipients and buffers for therapeutic formulations. [37,44–46]

4. Conclusion

Bundlemers have been computationally designed and characterized for their solution structure using a combination of SANS and NSE measurements. These investigations into inter-bundlemer interactions have shown that even though the bundlemers were designed to display a net neutral charge near pH 7.0, they behaved as complex colloids interacting via a balance of attraction and repulsion in low-ionic strength solution. Specifically, the bundlemer solution showed short-range order resulting in a mid-*Q* peak that was modeled using the Hayter-Penfold repulsive model. Addition of monovalent sodium chloride salt ions screened the repulsive interactions between bundlemers. Furthermore, NSE measurements of bundlemers confirmed freely diffusive bundlemer dynamics at high-*Q* comparable to the inter-bundlemer length scales. Interestingly, a small fraction of bundlemers always form bundlemer clusters, evidenced by a low-*Q* upturn. Electrostatic attraction between oppositely charged amino-acid side chains, hydrophobic interactions, and dispersive interactions at the bundlemer surface can all result in the formation of such clusters. Addition of phosphate buffer that contains multivalent ions increases the aggregation tendency of bundlemers via formation of ionic inter-bundlemer cross-links. Thus, bundlemers display a complicated interaction landscape due to the complexity of surface interactions, counterions from solution, and resulting patches that can form on an unequally charge-dissociated surface.

It is important to note that the peptide sequence and resulting net charge design and its distribution on the bundlemer surface can impact the interaction landscape between bundlemers. We have shown previously that in cases where designed attractive sites are not isotropic but rather site-specific and directional, kinetic pathway dependent self-assembly of bundlemers can be triggered into targeted 2D lattices or nanotubes under the right solution conditions, [13,47,48] which adds an extra layer of complexity to isotropic potentials that attempts to describe protein–protein interactions. Thus, the solution nanostructure not only depends on its solution conditions but can also be modulated via computational design of the bundlemer-forming sequence to create solution behavior that is similar to the interaction behavior of complex globular proteins. [2,11,34,49,50] The designability of bundlemers via computational design of side chains exposed to the solvent that mimics the complex multivalent surface of natural proteins is being actively explored and will shed light on such unexplored aspects of protein–protein interactions.

Proteins are different than traditional colloidal particles due to the rich interaction landscape afforded by multiple, oppositely charged side chains on their solvent-exposed surface as well as patchiness of interactions due to net charge and pattern. [11,12] Bundlemers formed by computationally designed peptides can function as model protein-mimicking colloids that are also synthetic materials that can be strategically linked to build arbitrary shaped self-assemblies. Importantly, the interaction landscape of the bundlemers can be transferred to its self-assemblies, as we have noted in our previous study of solution behavior of 1-d supramolecular rods of bundlemers that also showed a balance of inter-rod attraction and repulsion. [22] Thus, bundlemers offer a powerful template that can be employed to investigate the subtleties of protein–protein interactions and map the elusive protein–protein interaction landscape at the nanoscale.

CRediT authorship contribution statement

Nairiti J. Sinha: Conceptualization, Visualization, Investigation, Formal analysis, Data curation, Writing – original draft. **Rui Guo:** Investigation, Formal analysis, Data curation, Writing – original draft. **Rajkumar Misra:** Investigation, Formal analysis, Data curation. **Jeffrey Fagan:** Investigation, Formal analysis, Data curation, Writing – review & editing. **Antonio Faraone:** Investigation, Formal analysis, Data curation, Writing – review & editing. **Christopher J. Kloxin:** Writing – review & editing, Funding acquisition. **Jeffery G. Saven:** Writing – review & editing, Funding acquisition. **Grethe V. Jensen:** Writing – review & editing, Conceptualization, Validation, Supervision, Visualization. **Darrin J. Pochan:** Writing – review & editing, Conceptualization, Validation, Supervision, Resources, Funding acquisition, Visualization.

Declaration of Competing Interest

The authors declare that they have no known competing financial interests or personal relationships that could have appeared to influence the work reported in this paper.

Acknowledgements

This manuscript was prepared under cooperative agreement #370NANB17H302 from National Institute of Standards and Technology (NIST), U.S. Department of Commerce. We acknowledge the support of the NIST, U.S. Department of Commerce in providing the neutron research facilities used in this work. Access to vSANS was provided by the Center for High Resolution Neutron Scattering, a partnership between the National Institute of Standards and Technology and the National Science Foundation under Agreement No. DMR-2010792. Support for peptide design, synthesis, purification, and bundlemer rod formation was provided by the Department of Energy, Office of Basic Energy Sciences, Biomolecular Materials Program under grant No. DE-SC0019355 and DE-SC0019282. Samples were prepared for experiments at the NIST/IBBR Biomolecular Labeling Laboratory.

We thank Dr. Vivek Prabhu for access to the Dynamic Light Scattering instrument in his laboratory at NIST, Gaithersburg, MD. We would also like to thank Dr. Yun Liu and Dr. Paul Butler for their insights and comments that have benefitted the manuscript.

Disclaimer

The statements, findings, conclusions and recommendations are those of the authors and do not necessarily reflect the view of NIST or the U.S. Department of Commerce. Certain commercial equipment, instruments, materials, suppliers and software are identified in this paper to foster understanding. Such identification does not imply recommendation or endorsement by the NIST, nor does it imply that the materials or equipment identified are necessarily the best available for the purpose.

Appendix A. Supplementary material

Supplementary data to this article can be found online at https://doi.org/10.1016/j.jcis.2021.09.184.

References

[1] E.B. Sirota et al., Complete phase diagram of a charged colloidal system: A synchro- tron x-ray scattering study, Phys. Rev. Lett. 62 (1989) 1524–1527.
[2] L. Ianeselli et al., Protein−Protein Interactions in Ovalbumin Solutions Studied by Small-Angle Scattering: Effect of Ionic Strength and the Chemical Nature of Cations, J. Phys. Chem. B 114 (2010) 3776–3783.
[3] Y. Liu et al., Lysozyme Protein Solution with an Intermediate Range Order Structure, J. Phys. Chem. B 115 (2011) 7238–7247.
[4] S. Božič, T. Doles, H. Gradišar, R. Jerala, New designed protein assemblies, Curr. Opin. Chem. Biol. 17 (2013) 940–945.
[5] S.C. Glotzer, M.J. Solomon, N.A. Kotov, Self-assembly: From nanoscale to microscale colloids, AIChE J. 50 (2004) 2978–2985.
[6] Y. Liu, Intermediate scattering function for macromolecules in solutions probed by neutron spin echo, Phys. Rev. E 95 (2017) 020501.
[7] Y. Liu, Short-time dynamics of proteins in solutions studied by neutron spin echo, Curr. Opin. Colloid Interface Sci. 42 (2019) 147–156.
[8] J. Narayanan, X.Y. Liu, Protein Interactions in Undersaturated and Supersaturated Solutions: A Study Using Light and X-Ray Scattering, Biophys. J. 84 (2003) 523–532.
[9] C.R. Safinya, Biomolecular materials: Structure, interactions and higher order self- assembly, Colloids Surfaces A Physicochem. Eng. Asp. 128 (1997) 183–195.
[10] A. van Blaaderen, Colloids get complex, Nature 439 (2006) 545–546.
[11] A. Stradner, P. Schurtenberger, Potential and limits of a colloid approach to protein solutions, Soft Matter 16 (2020) 307–323.
[12] P.S. Sarangapani, S.D. Hudson, K.B. Migler, J.A. Pathak, The Limitations of an Exclusively Colloidal View of Protein Solution Hydrodynamics and Rheology, Biophys. J. 105 (2013) 2418–2426.
[13] H.V. Zhang et al., Computationally designed peptides for self-assembly of nanostructured lattices, Sci. Adv. 2 (2016) e1600307.
[14] M.J. Haider et al., Self-assembly and soluble aggregate behavior of computationally designed coiled-coil peptide bundles, Soft Matter 14 (2018) 5488–5496.
[15] D. Wu et al., Polymers with controlled assembly and rigidity made with click-functional peptide bundles, Nature 574 (2019) 658–662.
[16] N.J. Sinha et al., Recombinant expression of computationally designed peptide-bundlemers in Escherichia coli, J. Biotechnol. 330 (2021) 57–60.
[17] H. Kono, J.G. Saven, Statistical theory for protein combinatorial libraries. packing interactions, backbone flexibility, and the sequence variability of a main-chain structure11Edited by J. Thornton, J. Mol. Biol. 306 (2001) 607–628.
[18] J. Swift et al., Design of Functional Ferritin-Like Proteins with Hydrophobic Cavities, J. Am. Chem. Soc. 128 (2006) 6611–6619.
[19] J.E. Diaz et al., Computational design and selections for an engineered, thermostable terpene synthase, Protein Sci. 20 (2011) 1597–1606.
[20] M.J. Eibling et al., Controlling Association and Separation of Gold Nanoparticles with Computationally Designed Zinc-Coordinating Proteins, J. Am. Chem. Soc. 139 (2017) 17811–17823.
[21] K.W. Pulsipher et al., Thermophilic Ferritin 24mer Assembly and Nanoparticle Encapsulation Modulated by Interdimer Electrostatic Repulsion, Biochemistry 56 (2017) 3596–3606.
[22] N.J. Sinha et al., Polyelectrolyte character of rigid rod peptide bundlemer chains constructed via hierarchical self-assembly, Soft Matter 15 (2019) 9858–9870.
[23] D.A. Wellings, E. Atherton, [4] Standard Fmoc protocols, Methods in Enzymology 289 (1997) 44–67.
[24] S.R. Kline, Reduction and analysis of SANS and USANS data using IGOR Pro, J. Appl. Crystallogr. 39 (2006) 895–900.
[25] M. Doucet et al. SasView version 5.0. (2019). doi:10.5281/ZENODO.3011184
[26] R.T. Azuah et al., DAVE: A Comprehensive Software Suite for the Reduction, Visualization, and Analysis of Low Energy Neutron Spectroscopic Data, J. Res. Natl. Inst. Stand. Technol. 114 (2009) 341.
[27] P. Lindner, T.N. Zemb, X-rays and Light. Scattering Methods Applied to Soft Condensed Matter, Mater. Today 5 (2002) 38.
[28] M. Kotlarchyk, S.S. Chen, Analysis of small angle neutron scattering spectra from polydisperse interacting colloids, J. Chem. Phys. 79 (1983) 2461–2469.
[29] J.K. Percus, G.J. Yevick, Analysis of Classical Statistical Mechanics by Means of Collective Coordinates, Phys. Rev. 110 (1958) 1–13.
[30] J.B. Hayter, J. Penfold, An analytic structure factor for macroion solutions, Mol. Phys. 42 (1981) 109–118.
[31] J.-P. Hansen, J.B. Hayter, A rescaled MSA structure factor for dilute charged colloidal dispersions, Mol. Phys. 46 (1982) 651–656.
[32] H. Fischer, I. Polikarpov, A.F. Craievich, Average protein density is a molecular-weight-dependent function, Protein Sci. 13 (2009) 2825–2828.
[33] S.H. Kilcoyne, G.R. Mitchell, R. Cywinski, Temperature dependent SANS from ferritin and apoferritin, Phys. B Condens. Matter 180–181 (1992) 767–769.
[34] A. Stradner et al., Equilibrium cluster formation in concentrated protein solutions and colloids, Nature 432 (2004) 492–495.
[35] D.J. Winzor, Determination of the net charge (valence) of a protein: a fundamental but elusive parameter, Anal. Biochem. 325 (2004) 1–20.
[36] D. Qiu, T. Cosgrove, A.M. Howe, C.A. Dreiss, A Small-Angle X-ray Scattering Study of the Interactions in Concentrated Silica Colloidal Dispersions, Langmuir 22 (2006) 546–552.
[37] Y. Liu, E. Fratini, P. Baglioni, W.-R. Chen, S.-H. Chen, Effective Long-Range Attraction between Protein Molecules in Solutions Studied by Small Angle Neutron Scattering, Phys. Rev. Lett. 95 (2005) 118102.
[38] Y. Liu, W.-R. Chen, S.-H. Chen, Cluster formation in two-Yukawa fluids, J. Chem. Phys. 122 (2005) 044507.
[39] V.M. Prabhu, Counterion structure and dynamics in polyelectrolyte solutions, Curr. Opin. Colloid Interface Sci. 10 (2005) 2–8.
[40] H. Matsuoka, H. Murai, N. Ise, "'Ordered"' structure in colloidal silica particle suspensions as studied by small-angle x-ray scattering, Phys. Rev. B 37 (1988) 1368–1375.
[41] CRC Handbook of Chemistry and Physics, 86th Edition Edited by David R. Lide (National Institute of Standards and Technology). CRC Press (an imprint of Taylor and Francis Group): Boca Raton, FL. 2005. 2544 pp. $125.96. ISBN 0-8493-0486-5. J. Am. Chem. Soc. 128, 5585–5585 (2006).
[42] J.W. Bye, R.A. Curtis, Controlling Phase Separation of Lysozyme with Polyvalent Anions, J. Phys. Chem. B 123 (2019) 593–605.
[43] F. Roosen-Runge, F. Zhang, F. Schreiber, R. Roth, Ion-activated attractive patches as a mechanism for controlled protein interactions, Sci. Rep. 4 (2014) 7016.
[44] T.J. Kamerzell, R. Esfandiary, S.B. Joshi, C.R. Middaugh, D.B. Volkin, Protein–excipient interactions: Mechanisms and biophysical characterization applied to protein formulation development, Adv. Drug Deliv. Rev. 63 (2011) 1118–1159.
[45] D. Roberts et al., Specific Ion and Buffer Effects on Protein-Protein Interactions of a Monoclonal Antibody, Mol. Pharm. 12 (2015) 179–193.
[46] V. Vlachy, H.W. Blanch, J.M. Prausnitz, Liquid-liquid phase separations in aqueous solutions of globular proteins, AIChE J. 39 (1993) 215–223.
[47] Y. Tian, H.V. Zhang, K.L. Kiick, J.G. Saven, D.J. Pochan, Transition from disordered aggregates to ordered lattices: kinetic control of the assembly of a computationally designed peptide, Org. Biomol. Chem. 15 (2017) 6109–6118.
[48] Y. Tian et al., Nanotubes, Plates, and Needles: Pathway-Dependent Self-Assembly of Computationally Designed Peptides, Biomacromolecules 19 (2018) 4286–4298.
[49] F. Boué, F. Lefaucheux, M.C. Robert, I. Rosenman, Small angle neutron scattering study of lysozyme solutions, J. Cryst. Growth 133 (1993) 246–254.
[50] Y. Liu, Y. Xi, Colloidal systems with a short-range attraction and long-range repulsion: Phase diagrams, structures, and dynamics, Curr. Opin. Colloid Interface Sci. 39 (2019) 123–136.